Identification of DAXX As A Restriction Factor Of SARS-CoV-2 Through A CRISPR/Cas9 Screen

Alice Mac Kain[1,2], Ghizlane Maarifi[3], Sophie-Marie Aicher[2,4], Nathalie Arhel[3], Artem Baidaliuk[5], Thomas Vallet[1], Quang Dinh Tran[1,2], Alexandra Hardy[1], Maxime Chazal[4], Françoise Porrot[6], Molly OhAinle[7], Jared Carlson-Stevermer[8], Jennifer Oki[8], Kevin Holden[8], Etienne Simon-Lorière[5], Timothée Bruel[6], Olivier Schwartz[6], Nolwenn Jouvenet[4], Sébastien Nisole[3], Marco Vignuzzi[$1], Ferdinand Roesch*[1,9]

Author Affiliations:

1 Viral populations and pathogenesis, Institut Pasteur, CNRS UMR 3569, F-75015 Paris, France
2 Université de Paris, F-75013 Paris, France
3 Institut de Recherche en Infectiologie de Montpellier (IRIM), Université de Montpellier, CNRS, 34090 Montpellier, France
4 Virus sensing and signaling, Institut Pasteur, CNRS UMR 3569, F-75015 Paris, France
5 Evolutionary genomics of RNA viruses, Institut Pasteur, F-75015 Paris, France
6 Virus and Immunity, Institut Pasteur, CNRS UMR 3569, F-75015 Paris, France
7 Divisions of Human Biology, Fred Hutchinson Cancer Research Center, Seattle, United States
8 Synthego Corporation, 3565 Haven Avenue, Menlo Park, CA 94025
9 UMR 1282 ISP, INRAE Centre Val de Loire, Nouzilly, France

*** Corresponding author:**

Ferdinand Roesch.
ORCID: 0000-0003-0702-7778
Email: ferdinand.roesch@inrae.fr
Phone: +33 2 47 42 79 15
Current address: Equipe 3IMo ; UMR 1282 ISP - Infectiologie et Santé Publique
Centre de recherche INRAE Val de Loire
Route de Crotelles 37380 Nouzilly, France

$ Co-corresponding author:

Marco Vignuzzi
ORCID: 0000-0002-4400-771X
Email: marco.vignuzzi@pasteur.fr
Phone: 33 1 4568 8242

Abstract:

While interferon restricts SARS-CoV-2 replication in cell culture, only a handful of Interferon Stimulated Genes with antiviral activity against SARS-CoV-2 have been identified. Here, we describe a functional CRISPR/Cas9 screen aiming at identifying SARS-CoV-2 restriction factors. We identified DAXX, a scaffold protein residing in PML nuclear bodies known to limit the replication of DNA viruses and retroviruses, as a potent inhibitor of SARS-CoV-2 replication in human cells. Basal expression of DAXX was sufficient to limit the replication of the virus, and DAXX over-expression further restricted infection. In contrast with most of its previously described antiviral activities, DAXX-mediated restriction of SARS-CoV-2 was independent of the SUMOylation pathway. SARS-CoV-2 infection triggered the re-localization of DAXX to cytoplasmic sites of viral replication and led to its degradation. Together, these results demonstrate that DAXX is a potent restriction factor for SARS-CoV-2 and that the virus has evolved a mechanism to counteract its action.

Introduction. Severe Acute Respiratory Syndrome Coronavirus 2 (SARS-CoV-2) is the causative agent of COVID-19 and the third coronavirus to cause severe disease in humans after the emergence of SARS-CoV in 2002 and Middle East Respiratory Syndrome-related Coronavirus (MERS-CoV) in 2012. Since the beginning of the pandemic, SARS-CoV-2 has infected more than 140 million people and claimed 3 million lives. While the majority of infected individuals experience mild (or no) symptoms, severe forms of COVID-19 are associated with respiratory failure, shock and pneumonia. Innate immune responses play a key role in COVID-19 pathogenesis: immune exhaustion (1) and reduced levels of type-I and type-III interferon (IFN) have been observed in the plasma of severe COVID-19 patients (2,3). Imbalanced immune responses to SARS-CoV-2, with a low and delayed IFN response coupled to early and elevated levels of inflammation, have been proposed to be a major driver of COVID-19 (4,5). Neutralizing auto-antibodies against type-I IFN (6) and genetic alterations in several IFN pathway genes (7) have also been detected in critically ill COVID-19 patients. These studies highlight the crucial need to characterize the molecular mechanisms by which IFN pathway effectors may succeed, or fail, to control SARS-CoV-2 infection.

Although SARS-CoV-2 has been described to antagonize the IFN pathway by different mechanisms involving the viral proteins ORF3b, ORF9b ORF6, and nsp15 (8), detection of SARS-CoV-2 by the innate immune sensor Mda5 (9,10) leads to the synthesis of IFN and expression of IFN Stimulated Genes (ISGs) in human airway epithelial cells (4). IFN strongly inhibits SARS-CoV-2 replication when added in cell culture prior to infection (11,12) or when administered intranasally in hamsters (13), suggesting that some ISGs might have antiviral activity (14). However, relatively few ISGs with antiviral activity against SARS-CoV-2 have been identified so far. For instance, spike-mediated viral entry and fusion is restricted by LY6E (15,16) and IFITMs (17,18). Mucins have also been suggested in a recent pre-print to restrict viral entry (19). ZAP, which targets CpG dinucleotides in RNA viruses, also restricts SARS-CoV-2, albeit moderately (20). A recent overexpression screen identified 65 ISGs as potential inhibitors of SARS-CoV-2 (21), and found that BST-2/Tetherin is able to restrict viral budding, although this activity is counteracted by the viral protein ORF7a. The RNA helicase DDX42 was also shown to restrict several RNA viruses, including SARS-CoV-2 (22). We hypothesize that additional ISGs with antiviral activity against SARS-CoV-2 remain to be discovered. Other antiviral factors that are not induced by IFN may also inhibit SARS-CoV-2. While several whole-genome CRISPR/Cas9 screens identified host factors required for SARS-CoV-2 replication (23–28), none focused on antiviral genes.

Here, we performed a CRISPR/Cas9 screen designed to identify restriction factors for SARS-CoV-2, assessing the ability of 1905 ISGs to modulate SARS-CoV-2 replication in human epithelial lung cells. We report that the Death domain-associated protein 6 (DAXX), a scaffold protein residing in PML nuclear bodies (29) and restricting DNA viruses (30) and retroviruses (31,32), is a potent inhibitor of SARS-CoV-2 replication. SARS-CoV-2 restriction by DAXX is largely independent of the action of IFN, and unlike most of its other known activities, of the SUMOylation pathway. Within hours of infection, DAXX re-localizes to sites of viral replication in the cytoplasm, likely targeting viral

transcription. We also show that during the course of SARS-CoV-2 infection, DAXX is degraded, suggesting that SARS-CoV-2 developed a mechanism to counteract DAXX restriction.

Results.

A restriction factor-focused CRISPR/Cas9 screen identifies genes potentially involved in SARS-CoV-2 inhibition. To identify restriction factors limiting SARS-CoV-2 replication, we generated a pool of A549-ACE2 cells knocked-out (KO) for 1905 potential ISGs, using the sgRNA library we previously developed to screen HIV-1 restriction factors (33). This library includes more ISGs than most published libraries, as the inclusion criteria was less stringent (fold-change in gene expression in THP1 cells, primary CD4+ T cells or PBMCs $\geq$ 2). Transduced cells were selected by puromycin treatment, treated with IFNα and infected with SARS-CoV-2. Infected cells were immuno-labelled with a spike (S)-specific antibody and analyzed by flow cytometry. As expected (11,12), IFNα inhibited infection by 7-fold (**Fig. S1**). Infected cells were sorted based on S expression (**Fig. 1a**), and DNA was extracted from infected and non-infected control cells. Integrated sgRNA sequences in each cell fraction were amplified by PCR and sequenced by NGS. Statistical analyses using the MAGeCK package (34) led to the identification of sgRNAs significantly enriched or depleted in infected cells representing antiviral and proviral factors, respectively (**Fig. 1b**). Although our screen was not designed to explicitly study proviral factors, we did successfully identify the well-described SARS-CoV-2 co-factor cathepsin L (CTSL) (35), validating our approach. USP18, a negative regulator of the IFN signaling pathway (36), and ISG15, which favors Hepatitis C Virus replication (37), were also identified as proviral ISGs. In contrast, core IFN pathway genes such as the IFN receptor (IFNAR1), STAT1, and STAT2, were detected as antiviral factors, further validating our screening strategy. LY6E, a previously described inhibitor of SARS-CoV-2 entry (15,16), was also a significant hit. Moreover, our screen identified APOL6, IFI6, DAXX and HERC5, genes that are known to encode proteins with antiviral activity against other viruses (38–41), but had not previously been identified in the context of SARS-CoV-2 infection. For all these genes except APOL6, individual sgRNAs were consistently enriched (for antiviral factors) or depleted (for proviral factors) in the sorted population of infected cells, while non-targeting sgRNAs were not (**Fig. 1c**).

LY6E and DAXX display antiviral activity against SARS-CoV-2. To validate the ability of the identified hits to modulate SARS-CoV-2 replication in human cells, we generated pools of A549-ACE2 knocked-out (KO) cells for different genes of interest by electroporating a mix of 3 sgRNA/Cas9 ribonucleoprotein (RNP) complexes per gene target. Levels of gene editing were above 80% in all of the A549-ACE2 KO cell lines, as assessed by sequencing of the edited *loci* (**Table 1**). As controls, we used cells KO for IFNAR1, for the proviral factor CTSL or for the antiviral factor LY6E, as well as cells electroporated with non-targeting (NTC) sgRNAs/Cas9 RNPs. These different cell lines were then treated with IFNα and infected with SARS-CoV-2. Viral replication was assessed by measuring the levels of viral RNA in the supernatant of infected cells using RT-qPCR (**Fig. 2a**). In parallel, we titrated the levels of infectious viral particles released into the supernatant of infected cells (**Fig. 2b**). As expected, infection was significantly reduced in CTSL KO cells, confirming the proviral effect of this gene (35). Among the selected antiviral candidate genes, only 2 had a significant impact on SARS-CoV-2 replication: LY6E, and to an even greater degree, DAXX. Both genes restricted replication in absence of IFNα, an effect which was detectable at the level of viral RNA (8-fold and 42-fold reduction of infection, respectively, **Fig. 2a**) and of infectious virus (15-fold and 62-fold reduction, **Fig. 2b**). Based on available single-cell RNAseq datasets (42), DAXX is expected to be expressed in cell types relevant for SARS-CoV-2 such as lung epithelial cells, macrophages and T cells (**Fig. S3**).

In IFNα-treated cells. DAXX and LY6E KO led to a modest, but significant rescue of viral replication, which was particularly visible when measuring the levels of infectious virus by plaque assay titration (**Fig. 2b**), while the antiviral effect of IFNα treatment was completely abrogated in IFNAR1 KO cells, as expected (**Fig. 2c**). However, IFNα still had a strong antiviral effect on SARS-CoV-2 replication in both DAXX KO and LY6E KO cells (**Fig. 2c**). While DAXX and LY6E contribute to

105 the IFN-mediated restriction, this suggests that there are likely other ISGs contributing to this effect.
106 Although DAXX is sometimes referred to as an ISG, its expression is only weakly induced by IFN in
107 some human cell types (31,43). Consistent with this, we found little to no increase in DAXX expression
108 in IFNα-treated A549-ACE2 cells (**Fig. S2**). In addition, we tested the antiviral effect of DAXX on
109 several SARS-CoV-2 variants that have been suggested in a recent report to be partially resistant to
110 the antiviral effect of IFN (44). In these experiments, the 20I/501Y.V1 (UK), together with the
111 20J/501Y.V3 (Brazil) variant, were indeed less sensitive to IFN. DAXX, however, restricted all variants
112 to a similar level than the historical strain of SARS-CoV-2 (**Fig. 2d**). This suggest that while some
113 variants may have evolved towards IFN-resistance, they are still efficiently restricted by DAXX.
114 To further validate the antiviral activity of DAXX against SARS-CoV-2, we quantified the levels
115 of several viral transcripts in WT and DAXX KO cells (**Fig. 2e**). The levels of all the transcripts tested
116 strongly increased in DAXX KO cells (20 to 30-fold across all experiments). This further confirmed that
117 DAXX strongly interferes with SARS-CoV-2 replication and suggests that it may target viral
118 transcription, or an earlier step of the viral life cycle.
119
120 **DAXX restriction is SUMO-independent.** DAXX is a small scaffold protein that acts by recruiting
121 other SUMOylated proteins in nuclear bodies through its C-terminal SUMO-Interacting Motif (SIM)
122 domain (45). The recruitment of these factors is required for the effect of DAXX on various cellular
123 processes such as transcription and apoptosis, and on its antiviral activities (31,46–48). DAXX can
124 also be SUMOylated itself (49), which may be important for some of its functions. To investigate the
125 role of SUMOylation in DAXX-mediated SARS-CoV-2 restriction, we used overexpression assays to
126 compare the antiviral activity of DAXX WT with two previously described DAXX mutants (50). First, we
127 used a version of DAXX in which 15 lysine residues have been mutated to arginine (DAXX 15KR),
128 which is unable to be SUMOylated; and second, a truncated version of DAXX that is missing its C-
129 terminal SIM domain (DAXXΔSIM) (47) and is unable to interact with its SUMOylated partners. A549-
130 ACE2 were refractory to SARS-CoV-2 infection upon transfection with any plasmid, precluding us from
131 using this cell line. Instead, we transfected 293T-ACE2 cells, another SARS-CoV-2 permissive cell line
132 (18). Western blot (**Fig. S4a**) and flow cytometry (**Fig. S4b**) analyses showed that DAXX WT and
133 mutants were expressed to similar levels, with a transfection efficiency of 40 to 50% for all three
134 constructs.
135 We examined the effect of DAXX WT overexpression on the replication of SARS-CoV-2-
136 mNeonGreen (51) by microscopy. DAXX overexpression starkly reduced the number of infected cells
137 (**Fig. 3a**), revealing that DAXX-mediated restriction is not specific to A549-ACE2 cells. Using double
138 staining for HA-tagged DAXX and SARS-CoV-2, we found that most of the DAXX-transfected cells
139 were negative for infection, and conversely, that most of the infected cells did not express transfected
140 DAXX (**Fig. 3a**), indicating that DAXX imposes a major block to SARS-CoV-2 infection.
141 In order to quantify the antiviral effect of overexpressed DAXX WT and mutants, we assessed
142 the number of cells positive for the S protein (among transfected cells) by flow cytometry (**Fig. 3c-d**)
143 and the abundance of viral transcripts by qRT-PCR (**Fig. S4c**). DAXX WT, 15KR and ΔSIM all
144 efficiently restricted SARS-CoV-2 replication. Indeed, at 24 hours p.i., the proportion of infected cells
145 (among HA-positive cells) was reduced by 2 to 3-fold as compared to control transfected cells for all 3
146 constructs (**Fig. 3c**). This effect was less pronounced but still significant at 48 hours p.i. (**Fig. 3d**).
147 Moreover, DAXX overexpression led to a significant reduction of the levels of two different viral
148 transcripts (**Fig. S4c**), in line with our earlier results showing that DAXX targets viral transcription (**Fig.
149 2e**). Together, these results show that DAXX overexpression restricts SARS-CoV-2 transcription in a
150 SUMOylation-independent mechanism.
151
152 **SARS-CoV-2 infection triggers DAXX re-localization and degradation.** DAXX mostly localizes in
153 nuclear bodies (29), whereas SARS-CoV-2 replication occurs in the cytoplasm. We reasoned that
154 DAXX localization may be altered during the course of infection in order for the restriction factor to
155 exert its antiviral effect. To test this hypothesis, we infected 293T-ACE2 cells with SARS-CoV-2 and
156 used high-resolution confocal microscopy to study the localization of endogenous DAXX (**Fig. 4**). As
157 expected (29), DAXX mostly localizes in the nuclei of non-infected cells, forming discrete *foci*. 6h after

158 SARS-CoV-2 infection, DAXX begins to re-localize to the cytoplasm, although nuclear *foci* can still be
159 detected. At 24h post-infection, however, DAXX is completely depleted from nuclear bodies, and is
160 found almost exclusively in the cytoplasm of infected cells, in close association with SARS-CoV-2
161 dsRNA. Western blot analysis revealed that SARS-CoV-2 infection induces a marked decrease of total
162 DAXX expression in infected cells (**Fig. 5a**). This effect is visible at MOI 0.1, and almost complete
163 DAXX degradation can be observed at MOI 1. These results suggest that DAXX may be actively
164 targeted by SARS-CoV-2 for degradation during the course of infection. SARS-CoV-2 papain-like
165 protease (PLpro) is a possible candidate for this function, as it cleaves ISG15 from Mda5 (52) and
166 IRF3 (53). It was also shown that foot-and-mouth disease virus (FDMV) PLpro degrades DAXX (54).
167 We treated cells with GRL-0617, an inhibitor of SARS-CoV-2 PLpro (53). Strikingly, GRL-0617
168 treatment partially restores DAXX expression (**Fig. 5a**) and subcellular localization to nuclear bodies in
169 infected cells at 24h p.i. at MOI 0.1 (**Fig. 5b**). Although we cannot exclude that GRL-0617 treatment
170 may have an indirect effect on DAXX levels by inhibiting SARS-CoV-2 replication itself, this is unlikely
171 to be a major mitigating effect at 24h post-infection, particularly since imaging analysis reveals a
172 restoration of DAXX specifically in SARS-CoV-2 infected cells (**Fig. 5b**). Further work will be required
173 to uncover whether PLPro or a proteolytic product of the viral polyprotein chain degrades DAXX.
174
175 **Discussion.**
176
177 **Comparison with other screens.** The whole-genome CRISPR/Cas9 screens conducted to date on
178 SARS-CoV-2 infected cells mostly identified host factors necessary for viral replication (23–28) and
179 did not focus on antiviral genes, as did our screen. Two overexpression screens, however, identified
180 ISGs with antiviral activity against SARS-CoV-2 (16,21). In the first one, Pfaender *et al.* screened 386
181 ISGs for their antiviral activity against the endemic human coronavirus 229E, and identified LY6E as a
182 restriction factor inhibiting both 229E and SARS-CoV-2. Our screen also identified LY6E as a top hit
183 (**Fig.1**), further validating the findings of both studies. Four additional genes had significant p-values in
184 both Pfaender *et al.* and our work: IFI6, HERC5, OAS2 and SPSB1 (**Table S5-S6**). We showed that
185 knocking-out LY6E and DAXX only partially rescued SARS-CoV-2 replication in IFN-treated cells (**Fig.
186 2)**, suggesting that they contribute modestly to IFN-mediated restriction and that other IFN effectors
187 active against SARS-CoV-2 remain to be identified. For instance, other ISGs, such as IFITMs, inhibit
188 SARS-CoV-2 viral entry (17–19). In the second screen, Martin Sancho *et al.* tested 399 ISGs against
189 SARS-CoV-2. Among the 65 antiviral ISGs identified, they focused on BST-2/Tetherin, that targets
190 viral budding. BST-2/Tetherin was not a significant hit in our screen (**Table S5-6**). This discrepancy
191 can be easily explained by the fact that our screen relies on the sorting of S-positive cells, and is
192 therefore unable to detect late-acting antiviral factors. Of note, DAXX was absent from the ISG
193 libraries used by both overexpression screens, which explains why it was not previously identified as
194 an antiviral ISG for SARS-CoV-2. In contrast, our sgRNA library, by including 1905 genes, targeted a
195 wider set of ISGs and "ISG-like" genes, including genes like DAXX that are not (or only weakly)
196 induced by IFN in some cell types (31,43). Interestingly, IFN has a stronger effect on DAXX
197 expression levels in other mammals, including in some bat species (55). Future studies may
198 investigate whether DAXX orthologs of different species are also able to restrict SARS-CoV-2 and
199 whether DAXX participates in IFN-mediated viral restriction in these hosts.
200
201 **DAXX is a restriction factor for SARS-CoV-2.** Our CRISPR/Cas9 screen identifies DAXX as a
202 potent antiviral factor restricting the replication of SARS-CoV-2, acting independently of IFN and likely
203 targeting an early step of the viral life cycle such as transcription. DAXX fulfills all of the criteria
204 defining a *bona fide* SARS-CoV-2 restriction factor: knocking-out endogenous DAXX leads to an
205 enhanced viral replication (**Fig. 2**), while over-expression of DAXX restricts infection (**Fig. 3**). DAXX
206 co-localizes with viral dsRNA (**Fig. 4**) and SARS-CoV-2 antagonizes DAXX to some degree, as
207 evidenced by the degradation of DAXX induced by viral replication (**Fig. 5**). Although DAXX
208 expression is not upregulated by IFN (**Fig. S2**), basal levels of expression are sufficient for its antiviral
209 activity, as has been shown for other potent restriction factors. Single-cell RNAseq analyses (**Fig. S3**)

210 indicated that DAXX is expressed in cell types targeted by the virus in patients, such as lung epithelial
211 cells and macrophages.
212
213 **Mechanism of DAXX-mediated restriction.** DAXX is mostly known for its antiviral activity against
214 DNA viruses replicating in the nucleus, such as adenovirus 5 (AdV5) (56) and human papillomavirus
215 (HPV) (57). Most of these viruses antagonize PML and/or DAXX, which interacts with PML in nuclear
216 bodies (29). We show here that DAXX is also able to restrict a positive sense RNA virus that replicates
217 in the cytoplasm, which may represent a first step into establishing DAXX as a broad-spectrum
218 restriction factor. Recent studies have shown that DAXX inhibits the reverse transcription of HIV-1 in
219 the cytoplasm (31,32). Within hours of infection, DAXX subcellular localization was altered, with DAXX
220 accumulating in the cytoplasm and colocalizing with incoming HIV-1 capsids (32). Here, we observed
221 a similar phenomenon, with a rapid re-localization of DAXX from the nucleus to viral replication sites
222 (**Fig. 4**), where it likely exerts its antiviral effect. Early events in the replication cycle of both HIV-1 and
223 SARS-CoV-2, such as viral fusion or virus-induced stress, may thus trigger DAXX re-localization to the
224 cytoplasm. DAXX seems to inhibit SARS-CoV-2, however, by a distinct mechanism: whereas the
225 recruitment of SUMOylated partners through the SIM-domain is required for the effect of DAXX on
226 HIV-1 reverse transcription (31), it was not the case in the context of SARS-CoV-2 restriction. This
227 result was surprising, since DAXX has no enzymatic activity and rather acts as a scaffold protein
228 recruiting SUMOylated partners through its SIM domain (50). Some DAXX functions, such as
229 interaction with the chromatin remodeler ATRX (29), are however SIM-independent. Future work
230 should determine which DAXX domains and residues are required for its antiviral activity.
231
232 **Antagonism of DAXX by SARS-CoV-2.** SARS-CoV-2 replication triggers DAXX degradation (**Fig. 5**),
233 which likely represents an efficient antagonism strategy. Other viruses are also able to degrade DAXX:
234 for instance, the AdV5 viral protein E1B-55K targets DAXX for proteasomal degradation (56), and
235 FDMV PLpro directly degrades DAXX (54). We speculate that the SARS-CoV-2 proteases PLpro or
236 3C-like proteinase might be involved. Treatment of cells with GRL-0617, an inhibitor of PLpro, partially
237 prevented virus-induced DAXX degradation and restored DAXX localization to the nucleus. However,
238 this effect could be indirect, since GRL-0617 also blocks SARS-CoV-2 replication by preventing
239 polyprotein cleavage. Future work will be necessary to formally demonstrate the direct degradation of
240 DAXX by PLpro and to determine whether other viral strategies promote evasion from DAXX
241 restriction.
242
243 **Material & Methods.**
244
245 **Cells, viruses & plasmids.** HEK 293T (ATCC #CRL-11268) were cultured in MEM (Gibco #11095080)
246 complemented with 10% FBS (Gibco #A3160801) and 2 mM L-Glutamine (Gibco # 25030081). VeroE6 (ATCC
247 #CRL-1586), A549 (ATCC #CCL-185) and HEK 293T, both overexpressing the ACE2 receptor (A549-ACE2 and
248 HEK 293T-ACE2, respectively), were grown in DMEM (Gibco #31966021) supplemented with 10% FBS (Gibco
249 #A3160801), and penicillin/streptomycin (100 U/mL and 100 µg/mL, Gibco # 15140122). Blasticidin (10 µg/mL,
250 Sigma-Aldrich #SBR00022-10ML) was added for selection of A549-ACE2 and HEK 293T-ACE2. All cells were
251 maintained at 37°C in a 5% CO_2 atmosphere. Universal Type I Interferon Alpha (PBL Assay Science #11200-2)
252 was diluted in sterile-filtered PBS 1% BSA according to the activity reported by the manufacturer. The strains
253 BetaCoV/France/IDF0372/2020 (historical); hCoV-19/France/IDF-IPP11324/2020 (20I/501Y.V1 or UK); and
254 hCoV-19/France/PDL-IPP01065/2021 (20H/501Y.V2 or SA) were supplied by the National Reference Centre for
255 Respiratory Viruses hosted by Institut Pasteur and headed by Pr. Sylvie van der Werf. The human samples from
256 which the historical, UK and SA strains were isolated were provided by Dr. X. Lescure and Pr. Y. Yazdanpanah
257 from the Bichat Hospital, Paris, France; Dr. Besson J., Bioliance Laboratory, saint-Herblain France; Dr. Vincent
258 Foissaud, HIA Percy, Clamart, France, respectively. These strains were supplied through the European Virus
259 Archive goes Global (Evag) platform, a project that has received funding from the European Union's Horizon
260 2020 research and innovation programme under grant agreement #653316. The hCoV-19/Japan/TY7-501/2021
261 strain (20J/501Y.V3 or Brazil) was kindly provided by Jessica Vanhomwegen (Cellule d'Intervention Biologique
262 d'Urgence; Institut Pasteur). The mNeonGreen reporter SARS-CoV-2 was provided by Pei-Yong Shi (51). Viral
263 stocks were generated by infecting VeroE6 cells (MOI 0.01, harvesting at 3 dpi) using DMEM supplemented with
264 2% FBS and 1 µg/mL TPCK-trypsin (Sigma-Aldrich #1426-100MG). The Human Interferon-Stimulated Gene

265 CRISPR Knockout Library was a gift from Michael Emerman and is available on Addgene (Pooled Library
266 #125753). The plentiCRISPRv.2 backbone was ordered through Addgene (Plasmid #52961). pMD2.G and
267 psPAX2 were gifts from Didier Trono (Addgene #12259; #12260). pcDNA3.1 was purchased from Invitrogen.
268 Plasmids constructs expressing WT and mutant HA-tagged DAXX constructs were kindly provided by Hsiu-Ming
269 Shih (50).
270
271 **Antibodies.** For Western Blot, we used mouse anti-DAXX (diluted 1:1000, Abnova #7A11), rat anti-HA clone
272 3F10 (diluted 1:3000, Roche #11867423001) and mouse anti-GAPDH clone 6C5 (diluted 1:3000, Millipore
273 #FCMAB252F). Secondary antibodies were goat anti-mouse and anti-rabbit HRP-conjugates (diluted 1:5000,
274 GE Healthcare #NA931V and #NA934V). For immunofluorescence, we used rabbit anti-DAXX (diluted 1:50,
275 Proteintech #20489-1-AP) and mouse anti-dsRNA J2 (diluted 1:50, Scicons #10010200). Secondary antibodies
276 were goat anti-rabbit AF555 and anti-mouse AF488 (diluted 1:1000, ThermoFisher #A-21428 and #A-28175).
277 For flow sorting of infected cells, we used the anti-S2 H2 162 antibody (diluted 1:150), a kind gift from Dr. Hugo
278 Mouquet, (Institut Pasteur, Paris, France). Secondary antibody was donkey anti-mouse AF647 (diluted 1:1000,
279 Invitrogen #A31571). For FACS analysis, we used rat anti-HA clone 3F10 (diluted 1:100, Sigma #2158167001)
280 and mouse anti-dsRNA J2 (diluted 1:500, Scicons #10010200). Secondary antibodies were goat anti-rat AF647
281 and anti-mouse AF488 (diluted 1:1000, ThermoFisher #A-21247 #A-28175).
282
283 **Generation of CRISPR/Cas9 library cells.** HEK 293T cells were transfected with the sgRNA library plasmid
284 together with plasmids coding for Gag/Pol (R8.2) and for the VSVg envelope (pVSVg) using a ratio of 5:5:1 and
285 calcium phosphate transfection. Supernatants were harvested at 36h and 48h, concentrated 80-fold by
286 ultracentrifugation (22,000 g, 4°C for 1h) and pooled. To generate ISG KO library cells, $36x10^6$ A549-ACE2 cells
287 were seeded in 6 well plates (10^6 cells per well) 24h before transduction. For each well, 100 µL of concentrated
288 lentivector was diluted in 500 µL of serum-free DMEM, supplemented with 10 µg/mL of DEAE dextran (Sigma
289 #D9885). After 48h, transduced cells were selected by puromycin treatment for 20 days (1 µg/mL; Sigma
290 #P8833).
291
292 **CRISPR/Cas9 screen.** $4x10^7$ A549-ACE2 cells were treated with IFNα (200U/mL). 16h later, cells were infected
293 at a MOI of 1 in serum-free media complemented with TPCK-trypsin and IFNα (200 U/mL). After 90 min, the viral
294 inoculum was removed, and cells were maintained in DMEM containing 5% FBS and IFNα (200 U/mL). After
295 24h, cells were harvested and fixed for 15 min in Formalin 1%. Fixed cells were washed in cold FACS buffer
296 containing PBS, 2% Bovine Serum Albumin (Sigma-Aldrich #A2153-100G), 2 mM EDTA (Invitrogen #15575-
297 038) and 0.1% Saponin (Sigma-Aldrich #S7900-100G). Cells were incubated for 30 min at 4°C under rotation
298 with primary antibody diluted in FACS buffer. Incubation with the secondary antibody was performed during 30
299 min at 4°C under rotation. Stained cells were resuspended in cold sorting buffer containing PBS, 2% FBS, 25
300 mM Hepes (Sigma-Aldrich #H0887-100ML) and 5 mM EDTA. Infected cells were sorted on a BD FACS Aria
301 Fusion. Sorted and control (non-infected, not IFN-treated) cells were centrifugated (20 min, 2,000g) and
302 resuspended in lysis buffer (NaCl 300 mM, SDS 0.1%, EDTA 10 mM, EGTA 20 mM, Tris 10 mM) supplemented
303 with 1% Proteinase K (Qiagen #19133) and 1% RNAse A/T1 (ThermoFisher #EN0551) and incubated overnight
304 at 65°C. Two consecutive phenol-chloroform (Sigma #P3803-100ML) extractions were performed and DNA was
305 recovered by ethanol precipitation. Nested PCR was performed using the Herculase II Fusion DNA Polymerase
306 (Agilent, #600679) and the DNA oligos indicated in **Table S1**. PCR1 products were purified using QIAquick PCR
307 Purification kit (Qiagen #28104). PCR2 products were purified using Agencourt AMPure XP Beads (Beckman
308 Coulter Life Sciences #A63880). DNA concentration was determined using Qubit dsDNA HS Assay Kit (Thermo
309 Fisher #Q32854) and adjusted to 2 nM prior to sequencing. NGS was performed using the NextSeq 500/550
310 High Output Kit v2.5 75 cycles (Illumina #20024906).
311
312 **Screen analysis.** Reads were demultiplexed using bcl2fastq Conversion Software v2.20 (Illumina) and
313 fastx_toolkit v0.0.13. Sequencing adapters were removed using cutadapt v1.9.1 (58). The reference library was
314 built using bowtie2 v2.2.9 (59). Read mapping was performed with bowtie2 allowing 1 seed mismatch in --local
315 mode and samtools v1.9 (60). Mapping analysis and gene selection were performed using MAGeCK v0.5.6,
316 normalizing the data with default parameters. sgRNA and gene enrichment analyses are available in **Table S5-**
317 **S6**, respectively and full MAGeCK output at https://github.com/Simon-LoriereLab/crispr_isg_sarscov2.
318
319 **Generation of multi-guide gene knockout cells.** 3 sgRNAs per gene were designed (**Table S2**). 10 pmol of
320 NLS-Sp.Cas9-NLS (SpCas9) nuclease (Aldevron #9212) was combined with 30 pmol total synthetic sgRNA (10
321 pmol for each sgRNA) (Synthego) to form RNPs in 20 µL total volume with SE Buffer (Lonza #V5SC-1002). The
322 reaction was incubated at room temperature for 10 min. $2x10^5$ cells per condition were pelleted by centrifugation

323 at 100*g* for 3 min, resuspended in SE buffer and diluted to $2x10^4$ cells/µL. 5 µL of cell solution was added to the
324 pre-formed RNP solution and gently mixed. Nucleofections were performed on a Lonza HT 384-well nucleofector
325 system (Lonza #AAU-1001) using program CM-120. Immediately following nucleofection, each reaction was
326 transferred to a 96-well plate containing 200 µL of DMEM 10% FBS ($5x10^4$ cells per well). Two days post-
327 nucleofection, DNA was extracted using DNA QuickExtract (Lucigen #QE09050). Cells were lysed in 50 µL of
328 QuickExtract solution and incubated at 68°C for 15 min followed by 95°C for 10 min. Amplicons were generated
329 by PCR amplification using NEBNext polymerase (NEB #M0541) or AmpliTaq Gold 360 polymerase
330 (ThermoFisher #4398881) and the primers indicated in **Table S3**. PCR products were cleaned-up and analyzed
331 by Sanger sequencing. Sanger data files and sgRNA target sequences were input into Inference of CRISPR
332 Edits (ICE) analysis https://ice.synthego.com/#/ to determine editing efficiency and to quantify generated indels
333 (61). Percentage of alleles edited is expressed as an ice-d score.
334
335 **SARS-CoV-2 infection assays.** A549-ACE2 cells were infected by incubating the virus for 1h with the cells
336 maintained in DMEM supplemented with 1 µg/ml TPCK-trypsin (Sigma #4370285). The viral input was then
337 removed and cells were kept in DMEM supplemented with 2% FBS. For 293T-ACE2 cells, infections were
338 performed without TPCK-trypsin. All experiments involving infectious material were performed in Biosafety Level
339 3 facilities in compliance with Institut Pasteur's guidelines and procedures.
340
341 **Hit validation.** $2.5x10^4$ A549-ACE2 KO cells were seeded in 96-well plates 18h before the experiment. Cells
342 were treated with IFNα and infected as described above. At 72h post-infection, supernatants and cellular
343 monolayers were harvested in order to perform qRT-PCR and plaque assay titration. Infectious supernatants
344 were heat-inactivated at 80°C for 10 min. For intracellular RNA, cells were lysed in a mixture of Trizol Reagent
345 (Invitrogen #15596018) and PBS at a ratio of 3:1. Total RNA was extracted using the Direct-zol 96 RNA kit
346 (Zymo Research #R2056) or the Direct-zol RNA Miniprep kit (Zymo Research #R2050). qRT-PCR was
347 performed either directly on the inactivated supernatants or on extracted RNA using the Luna Universal One-
348 Step RT-qPCR Kit (NEB #E3005E) in a QuantStudio 6 thermocycler (Applied Biosystems) or in a StepOne Plus
349 thermocycler (Applied Biosystems). Primers used are described in **Table S4**. Cycling conditions were the
350 following: 10 min at 55°C, 1 min at 95°C and 40 cycles of 95°C for 10s and 60°C for 1 min. Results are
351 expressed as PFU equivalents/mL as the standard curve was performed by diluting RNA extracted from a viral
352 stock with a known titer. For plaque assay titration, VeroE6 cells were seeded in 24-well plates (10^5 cells per
353 well) and infected with serial dilutions of infectious supernatant diluted in DMEM during 1h at 37°C. After
354 infection, 0.1% agarose semi-solid overlays were added. At 72h post-infection, cells were fixed with Formalin 4%
355 (Sigma #HT501128-4L) and plaques were visualized using crystal violet coloration.
356
357 **Overexpression assay.** $2x10^5$ 293T-ACE2 cells were seeded in a 24-well plate 18h before experiment. Cells
358 were transfected with 500 ng of plasmids expressing HA-DAXX WT, HA-DAXX 15KR and HA-DAXXΔSIM
359 plasmids, using Fugene 6 (Promega # E2691), following the manufacturer's instructions. HA-NRB1 was used as
360 negative control. After 24h cells were infected at the indicated MOI in DMEM 2% FBS. When indicated, cells
361 were treated with 10 mM of remdesivir (MedChemExpress #HY-104077) at the time of infection. For flow
362 cytometry analysis, cells were fixed with 4% formaldehyde and permeabilized in a PBS 1% BSA 0.025% saponin
363 solution for 30 min prior to staining with corresponding antibodies for 1h at 4°C diluted in the permeabilization
364 solution. Samples were acquired on a BD LSR Fortessa and analyzed using FlowJo. Total RNA was extracted
365 using a RNeasy Mini kit and submitted to DNase treatment (Qiagen). RNA concentration and purity were
366 evaluated by spectrophotometry (NanoDrop 2000c, ThermoFisher). In addition, 500 ng of RNA were reverse
367 transcribed with both oligo dT and random primers, using a PrimeScript RT Reagent Kit (Takara Bio) in a 10 mL
368 reaction. Real-time PCR reactions were performed in duplicate using Takyon ROX SYBR MasterMix blue dTTP
369 (Eurogentec) on an Applied Biosystems QuantStudio 5 (ThermoFisher). Transcripts were quantified using the
370 following program: 3 min at 95°C followed by 35 cycles of 15s at 95°C, 20s at 60°C, and 20s at 72°C. Values for
371 each transcript were normalized to expression levels of RPL13A. The primers used are indicated in **Table S4**.
372
373 **Western blot.** Cell lysates were prepared using RIPA lysis and extraction buffer (ThermoFisher #89901). Protein
374 concentration was determined using Bradford quantification. Proteins were denaturated using 4X Bolt LDS
375 Sample Buffer (Invitrogen) and 10X Bolt Sample Reducing Agent (Invitrogen). 40 µg of proteins were separated
376 on Bolt 4-12% Bis-Tris Mini Protein Gels (Invitrogen) and transferred on membranes using the iBlot Transfer
377 Stack PVDF mini (Invitrogen) and an iBlot Dry Blotting System (Invitrogen). Membranes were blocked with 5%
378 BSA in PBS (blocking buffer) and incubated with primary antibodies diluted in blocking buffer. Membranes were
379 washed and incubated with secondary antibodies diluted in blocking buffer. SuperSignal West Pico PLUS

Chemiluminescent Substrate (ThermoFisher #34579) was added on the membranes and pictures were taken on a myECL Imager (ThermoFisher).

Microscopy Immunolabeling and Imaging. 293T-ACE2 cells were cultured and infected with SARS-CoV-2 as described above. When indicated, cells were treated with 50 mg/mL of GRL-0617 (MedChemExpress #HY-117043), a specific inhibitor of SARS-CoV-2 PLpro (53), at the time of infection.
Cultures were rinsed with PBS and fixed with 4% paraformaldehyde (electronic microscopy grade; Alfa Aesar) in PBS for 10 min at room temperature, treated with 50 mM NH4Cl for 10 min, permeabilized with 0.5% Triton X-100 for 15 min, and blocked with 0.3% BSA for 10 min. Cells were incubated with primary and secondary antibodies for 1h and 30 min, respectively, in a moist chamber. Nuclei were labeled with Hoechst dye (Molecular Probes). Images were acquired using a LSM700 (Zeiss) confocal microscope equipped with a 63X objective or by Airyscan LSM800 (Zeiss). Image analysis was performed using ImageJ.

Single-cell RNAseq analysis. Single cell RNAseq analysis were performed in the BioTuring Browser Software (v2.8.42) developed by BioTuring, using a dataset made available by Liao *et al.* (42) (ID: GSE145926). All processing steps were done by BioTuring Browser (62). Cells with less than 200 genes and mitochondrial genes higher than 10% were excluded from the analysis.

Statistical analysis. GraphPad Prism was used for statistical analyses. Linear models were computed using Rstudio.

Figures.

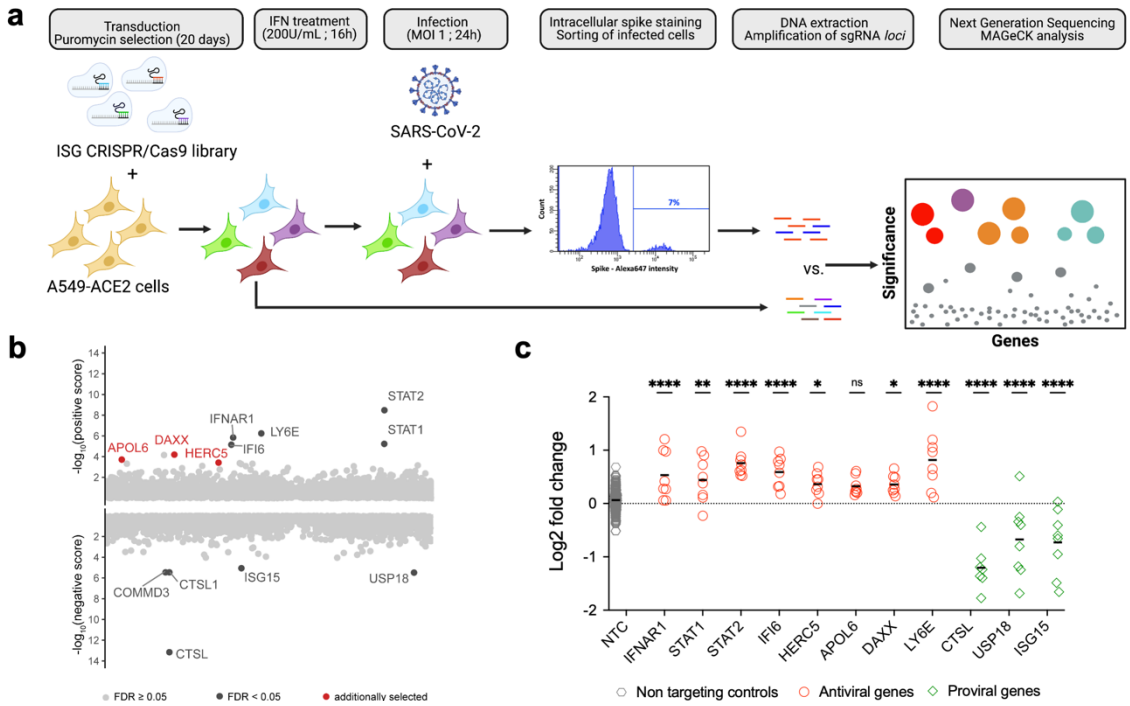

Figure 1: ISG-focused CRISPR/Cas9 screening approach to identify restriction factors for SARS-CoV-2. a: CRISPR/Cas9 screen outline. A549-ACE2 cells were transduced with lentivectors encoding the ISG CRISPR/Cas9 library and selected by puromycin treatment for 20 days. Library cells were then pre-treated with 200 U/mL of IFNα for 16 hours, and infection with SARS-CoV-2 at MOI 1. 24 hours post infection, infected cells were fixed with formalin treatment, permeabilized by saponin treatment and stained with a monoclonal anti-spike antibody. After secondary staining, infected cells were sorted and harvested. Non-infected, non-IFNα treated cells were harvested as a control. DNA was extracted from both cellular fractions and sgRNA *loci* amplification was carried out by PCR. Following NGS, bio-informatic analysis using the MAGeCK package was conducted. **b: Screen results**. By taking into account the enrichment ratios of each of the 8 different sgRNAs for every gene, the MAGeCK analysis provides a modified robust rank aggregation (α-RRA) score, with further one-sided significance testing. A positive score is assigned to KOs enriched in infected cells (*i.e.* restriction factor, represented in the top fraction of the graph) and a negative score is assigned to KOs depleted in infected cells (*i.e.* proviral factors, represented in the bottom portion of the graph). Gene with an FDR < 0.05 are represented in black. 3 genes with a FDR > 0.05, but with a p-value < 0.005 were additionally selected and are represented in red. **c: Individual sgRNA enrichment.** For the indicated genes, the enrichment ratio of the 8 sgRNAs present in the library was calculated as the MAGeCK normalized read counts in infected cells divided by those in the original pool of cells and is represented in log2 fold change. As a control, the enrichment ratios of the 200 non-targeting control sgRNAs (NTCs) are also represented, merged together in one NTC for visualization purposes only. Statistics: one-way ANOVA, ns = p-value > 0.05, * = p-value < 0.05, ** = p-value < 0.01, **** = p-value < 0.0001.

428 **Table 1: Gene editing efficiency.**
429

Gene	% of alleles edited
LY6E	97
DAXX	82
APOL6	99
HERC5	97
CTSL	87
IFI6	83
IFNAR1	79

430

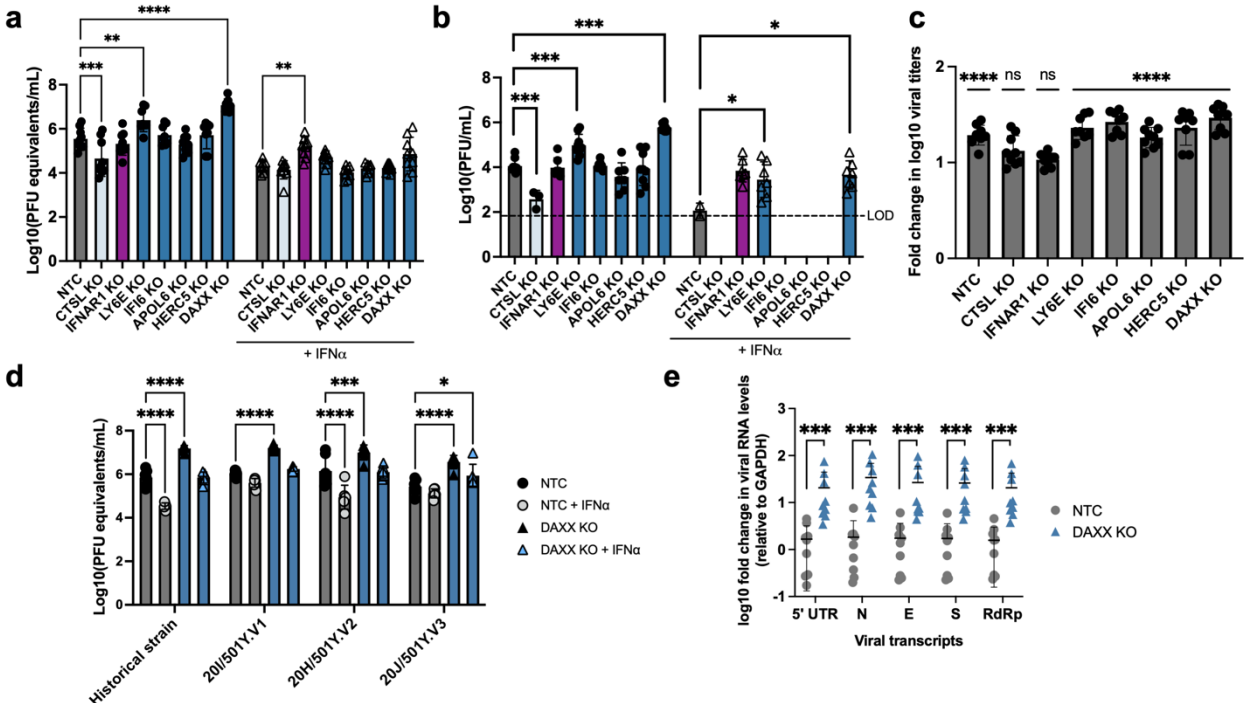

Figure 2: DAXX is a restriction factor for SARS-CoV-2. A-C: Antiviral activity of ISGs against SARS-CoV-2. A549-ACE2 knocked-out for the indicated genes were generated using a multi-guide approach, leading to pools of KO cells with a high frequency of indels. KO cells were pre-treated with 0 (circles) or 200 (triangles) U/mL of IFNα 24h prior to triplicate infection with SARS-CoV-2 (MOI 0.1). Supernatants were harvested at 72h post infection. The mean of three independent experiments, with infections carried out in triplicate, is shown. **a:** For the titration of RNA levels, supernatants were heat inactivated prior to quantification by qRT-PCR. Serial dilutions of a stock of known infectious titer was used as a standard (PFU equivalents/mL). Statistics: 2-way ANOVA, * = p-value < 0.05, ** = p-value < 0.01, *** = p-value < 0.001, **** = p-value < 0.0001. **b:** For the titration of infectious virus levels by plaque assay, supernatants were serially diluted and used to infect VeroE6 cells. Plaques formed after 3 days of infection were quantified using crystal violet coloration. Statistics: Dunnett's test on a linear model, * p-value < 0.05, ** p-value < 0.01, *** p-value < 0.001. **c:** For each of the indicated KO, the data shown in A is represented as fold change in log10 titers (*i.e.* the triplicate log10 titers of the non-treated condition divided by the mean of the triplicate log10 titers IFNα-treated condition, n=3). Statistics: 2-way ANOVA, ns = p-value > 0.05, **** = p-value < 0.001. **d:** A549-ACE2 WT or DAXX KO cells were infected in triplicates at an MOI of 0.1 with the following SARS-CoV-2 strains: BetaCoV/France/IDF0372/2020 (historical strain) ; hCoV-19/France/IDF-IPP11324/2020 (20I/501Y.V1, sometimes referred to as United Kingdom or B.1.1.7) ; hCoV-19/France/PDL-IPP01065/2021 (20H/501Y.V2, sometimes referred to as South Africa or B.1.351) ; hCoV-19/Japan/TY7-501/2021 (20J/501Y.V3, sometimes referred to as Brazil or P.1). Supernatants were harvested at 72h post infection. Supernatants were heat inactivated prior to quantification by qRT-PCR. Serial dilutions of a stock of known infectious titer was used as a standard (PFU equivalents/mL). The mean of two independent experiments, with infections carried out in triplicate, is shown. Statistics: 2-way ANOVA, * = p-value < 0.05, *** = p-value < 0.001, **** = p-value < 0.0001. **e:** A549-ACE2 WT or DAXX KO were infected in triplicates with SARS-CoV-2 at a MOI of 0.1. After 72h of infection, cell monolayers were harvested and cellular RNAs were extracted. The levels of each of the indicated viral transcripts were quantified by qRT-PCR and normalized to GAPDH levels. Fold change in DAXX KO cells compared to the average of control cells is represented. 3 independent experiments are shown and taken into account as fixed effects in a linear model. Statistics: Dunnett's test on a linear model, * p-value < 0.05, ** p-value < 0.01, *** p-value < 0.001.

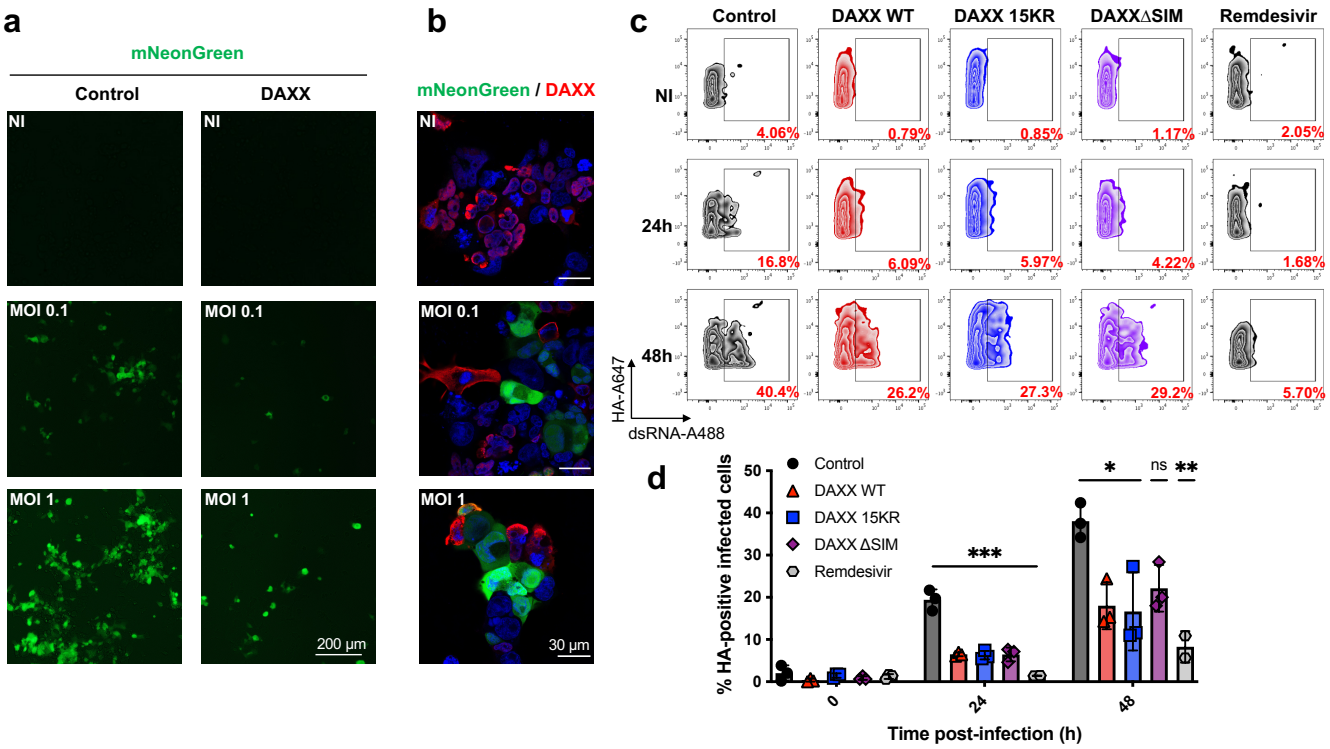

Figure 3: DAXX restriction of SARS-CoV-2 is SUMOylation independent. A-B: DAXX overexpression restricts SARS-CoV-2. 293T-ACE2 cells were transfected with DAXX WT. 24h after transfection, cells were infected with the mNeonGreen fluorescent reporter SARS-CoV-2 at the indicated MOI. Cells were either visualized with an EVOS fluorescence microscope (**a**) or stained with an HA-antibody detecting DAXX and imaged by confocal microscopy (**b**). Scale bars correspond to 200 µm (**a**) and 30 µm (**b**) **c-d: DAXX mutants are still able to restrict SARS-CoV-2**. 293T-ACE2 cells were transfected with HA-DAXX WT ; H-ADAXX 15KR ; HA-DAXXΔSIM ; or with HA-NRB1 as negative control plasmid. 24h after transfection, cells were infected with SARS-CoV-2 at an MOI of 0.1. When indicated, cells were treated with remdesivir at the time of infection. After 24 or 48h, infected cells were double-stained recognizing dsRNA (to read out infection) and HA (to read out transfection efficiency) and acquired by flow cytometry. The percentage of infected cells among HA-positive (transfected) cells for one representative experiments is shown in **c**, for the mean of 3 independent experiments in **d**. Statistics: one-way ANOVA Holm corrected, ns = p-value > 0.05, * = p-value < 0.05, ** = p-value < 0.01, *** = p-value < 0.001.

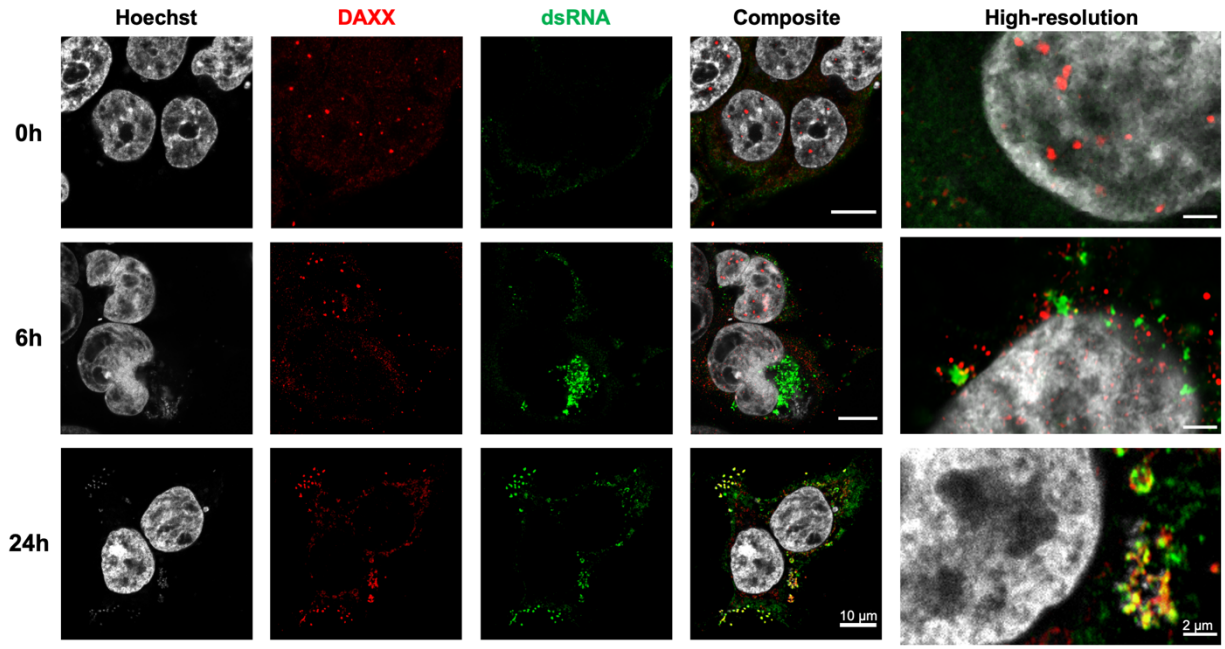

Figure 4: SARS-CoV-2 infection induces DAXX cytoplasmic re-localization to sites of viral replication. 293T-ACE2 cells were infected with SARS-CoV-2 at the indicated MOI 1. 24h post-infection, cells were labelled with Hoescht and with antibodies against dsRNA (detecting viral RNA, in green) and HA (detecting DAXX, in red). When indicated, the high-resolution Airyscan mode was used. Scale bars correspond to 10 µm for confocal images, and 2 µm for the high-resolution images.

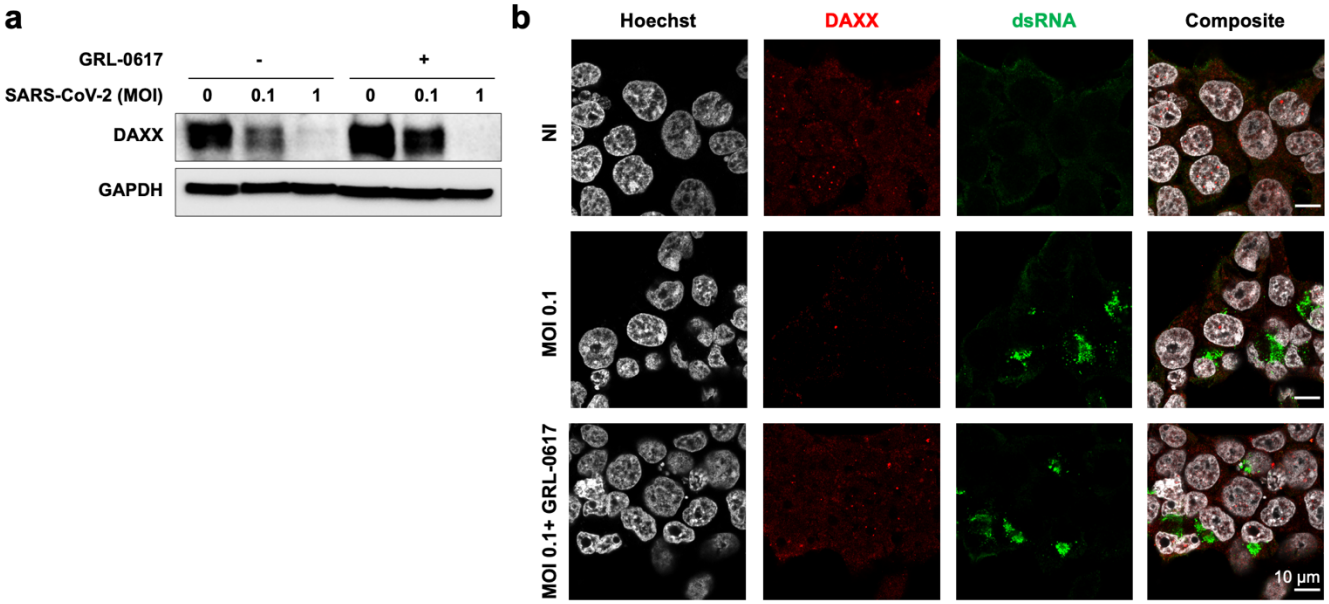

Figure 5: SARS-CoV-2 antagonizes DAXX restriction. a: DAXX degradation after infection. 293T-ACE2 cells were infected with SARS-CoV-2 at the indicated MOI. After 24h, cells were harvested and levels of DAXX and GAPDH were analyzed by Western Blot. When indicated, cells were treated with the viral protease inhibitor GRL-0617 at the time of infection. **b: GRL-0617 treatment partially reverses DAXX re-localization and expression.** 293T-ACE2 cells were infected with SARS-CoV-2 at the indicated MOI 0.1. 24h post-infection, cells were labelled with Hoescht and with antibodies against dsRNA (detecting viral RNA, in green) and HA (detecting DAXX, in red). When indicated, cells were treated with the viral protease inhibitor GRL-0617 at the time of infection. Scale bars correspond to 10 µm.

Acknowledgements. We thank the Cytometry Platform, Center for Technological Resources and Research, Institut Pasteur, for cell sorting experiments. This work was funded by the Institut Pasteur Coronavirus Task Force, CNRS (UMR 3569) and by the ANR (ANR-20-COVI-000, projects IDISCOVR to M.V. and Alpha-COV to S.N.). A.M.K. is supported by a grant of the French Ministry of Higher Education, Research and Innovation. G.M. is supported by a grant from the Agence nationale de recherches sur le sida et les hépatites virales (ANRS). We thank Michael Emerman, Daniel Marc and Ignacio Caballero-Posadas for helpful comments on the manuscript. Illustrative figures in this manuscript were created with BioRender.com.

Contributions. F.R. designed the research project. F.R. and M.V. secured the funding for the study. A.M.K., S.M.A., A.H., N.A., S.N., G.M., D.Q.T., M.C., T.V. and F.R. performed and analyzed the *in vitro* experiments. F.P. produced the stocks of lentivirus. J.C.S., J.O. and K.H. generated and validated KO cell lines. T.B. performed the single-cell RNAseq data analysis. A.B. and E.S.L. performed the bio-informatic analyses of the CRISPR/Cas9 screen. M.O., T.B., O.S., N.J., S.N., and M.V. analyzed the data and supervised the project. A.M.K. and F.R. wrote the manuscript. All authors edited the manuscript.

Competing Interests: J.C.S., J.O. and K.H. are employees and shareholders from Synthego Corporation.

Correspondence and requests for materials should be addressed to M.V. or F.R.

Data availability: Raw NGS data was deposited to the NCBI GEO portal and is accessible with the number GSE173418.

References.

1. Ruetsch C, Brglez V, Crémoni M, Zorzi K, Fernandez C, Boyer-Suavet S, et al. Functional Exhaustion of Type I and II Interferons Production in Severe COVID-19 Patients. Front Med. 2021 Jan 27;7:603961.
2. Hadjadj J, Yatim N, Barnabei L, Corneau A, Boussier J, Smith N, et al. Impaired type I interferon activity and inflammatory responses in severe COVID-19 patients. Science. 2020 Aug 7;369(6504):718–24.
3. Combes AJ, Courau T, Kuhn NF, Hu KH, Ray A, Chen WS, et al. Global absence and targeting of protective immune states in severe COVID-19. Nature. 2021 Mar 1;591(7848):124–30.
4. Blanco-Melo D, Nilsson-Payant BE, Liu W-C, Uhl S, Hoagland D, Møller R, et al. Imbalanced Host Response to SARS-CoV-2 Drives Development of COVID-19. Cell. 2020 May;181(5):1036-1045.e9.
5. Galani I-E, Rovina N, Lampropoulou V, Triantafyllia V, Manioudaki M, Pavlos E, et al. Untuned antiviral immunity in COVID-19 revealed by temporal type I/III interferon patterns and flu comparison. Nat Immunol. 2021 Jan;22(1):32–40.
6. Bastard P, Rosen LB, Zhang Q, Michailidis E, Hoffmann H-H, Zhang Y, et al. Autoantibodies against type I IFNs in patients with life-threatening COVID-19. Science. 2020 Oct 23;370(6515):eabd4585.
7. Zhang Q, Bastard P, Liu Z, Le Pen J, Moncada-Velez M, Chen J, et al. Inborn errors of type I IFN immunity in patients with life-threatening COVID-19. Science. 2020 Oct 23;370(6515):eabd4570.
8. Sa Ribero M, Jouvenet N, Dreux M, Nisole S. Interplay between SARS-CoV-2 and the type I interferon response. PLOS Pathog. 2020 Jul 29;16(7):e1008737.
9. Rebendenne A, Chaves Valadão AL, Tauziet M, Maarifi G, Bonaventure B, McKellar J, et al. SARS-CoV-2 Triggers an MDA-5-Dependent Interferon Response Which Is Unable To Control Replication in Lung Epithelial Cells. J Virol. 2021 Mar 25;95(8):e02415-20.

548 10. Yin X, Riva L, Pu Y, Martin-Sancho L, Kanamune J, Yamamoto Y, et al. MDA5 Governs the
549 Innate Immune Response to SARS-CoV-2 in Lung Epithelial Cells. Cell Rep. 2021 Jan;34(2):108628.
550 11. Felgenhauer U, Schoen A, Gad HH, Hartmann R, Schaubmar AR, Failing K, et al. Inhibition of
551 SARS–CoV-2 by type I and type III interferons. J Biol Chem. 2020 Oct 9;295(41):13958–64.
552 12. Lokugamage KG, Hage A, de Vries M, Valero-Jimenez AM, Schindewolf C, Dittmann M, et al.
553 Type I Interferon Susceptibility Distinguishes SARS-CoV-2 from SARS-CoV. J Virol. 2020 Nov
554 9;94(23):e01410-20.
555 13. Hoagland DA, Møller R, Uhl SA, Oishi K, Frere J, Golynker I, et al. Leveraging the antiviral
556 type I interferon system as a first line of defense against SARS-CoV-2 pathogenicity. Immunity. 2021
557 Jan;S1074761321000406.
558 14. Busnadiego I, Fernbach S, Pohl MO, Karakus U, Huber M, Trkola A, et al. Antiviral Activity of
559 Type I, II, and III Interferons Counterbalances ACE2 Inducibility and Restricts SARS-CoV-2. mBio.
560 2020 Oct 27;11(5):e01928-20.
561 15. Zhao X, Zheng S, Chen D, Zheng M, Li X, Li G, et al. LY6E Restricts Entry of Human
562 Coronaviruses, Including Currently Pandemic SARS-CoV-2. J Virol. 2020 Aug 31;94(18):e00562-20.
563 16. Pfaender S, Mar KB, Michailidis E, Kratzel A, Boys IN, V'kovski P, et al. LY6E impairs
564 coronavirus fusion and confers immune control of viral disease. Nat Microbiol. 2020 Nov;5(11):1330–
565 9.
566 17. Shi G, Kenney AD, Kudryashova E, Zani A, Zhang L, Lai KK, et al. Opposing activities of
567 IFITM proteins in SARS-CoV-2 infection. EMBO J. 2021 Feb 1;40(3):e106501.
568 18. Buchrieser J, Dufloo J, Hubert M, Monel B, Planas D, Rajah MM, et al. Syncytia formation by
569 SARS-CoV-2-infected cells. EMBO J. 2020 Dec;39(23).
570 19. Biering SB, Sarnik SA, Wang E, Zengel JR, Sathyan V, Nguyenla X, et al. Genome-wide,
571 bidirectional CRISPR screens identify mucins as critical host factors modulating SARS-CoV-2
572 infection. bioRxiv. 2021 Jan 1;2021.04.22.440848.
573 20. Nchioua R, Kmiec D, Müller JA, Conzelmann C, Groß R, Swanson CM, et al. SARS-CoV-2 Is
574 Restricted by Zinc Finger Antiviral Protein despite Preadaptation to the Low-CpG Environment in
575 Humans. mBio. 2020 Oct 27;11(5):e01930-20.
576 21. Martin-Sancho L, Lewinski MK, Pache L, Stoneham CA, Yin X, Becker ME, et al. Functional
577 Landscape of SARS-CoV-2 Cellular Restriction. Mol Cell. 2021 Apr 13;
578 22. Bonaventure B, Rebendenne A, Garcia de GF, McKellar J, Tauziet M, Chaves Valadão AL, et
579 al. A genome-wide CRISPR/Cas9 knock-out screen identifies the DEAD box RNA helicase DDX42 as
580 a broad antiviral inhibitor. bioRxiv. 2020 Jan 1;2020.10.28.359356.
581 23. Hoffmann H-H, Sánchez-Rivera FJ, Schneider WM, Luna JM, Soto-Feliciano YM, Ashbrook
582 AW, et al. Functional interrogation of a SARS-CoV-2 host protein interactome identifies unique and
583 shared coronavirus host factors. Cell Host Microbe. 2021 Feb;29(2):267-280.e5.
584 24. Daniloski Z, Jordan TX, Wessels H-H, Hoagland DA, Kasela S, Legut M, et al. Identification of
585 Required Host Factors for SARS-CoV-2 Infection in Human Cells. Cell. 2021 Jan;184(1):92-105.e16.
586 25. Wei J, Alfajaro MM, DeWeirdt PC, Hanna RE, Lu-Culligan WJ, Cai WL, et al. Genome-wide
587 CRISPR Screens Reveal Host Factors Critical for SARS-CoV-2 Infection. Cell. 2021 Jan;184(1):76-
588 91.e13.
589 26. Schneider WM, Luna JM, Hoffmann H-H, Sánchez-Rivera FJ, Leal AA, Ashbrook AW, et al.
590 Genome-Scale Identification of SARS-CoV-2 and Pan-coronavirus Host Factor Networks. Cell. 2021
591 Jan;184(1):120-132.e14.
592 27. Wang R, Simoneau CR, Kulsuptrakul J, Bouhaddou M, Travisano KA, Hayashi JM, et al.
593 Genetic Screens Identify Host Factors for SARS-CoV-2 and Common Cold Coronaviruses. Cell. 2021
594 Jan;184(1):106-119.e14.
595 28. Baggen J, Persoons L, Vanstreels E, Jansen S, Van Looveren D, Boeckx B, et al. Genome-wide
596 CRISPR screening identifies TMEM106B as a proviral host factor for SARS-CoV-2. Nat Genet. 2021

597 Apr;53(4):435–44.
598 29. Tang J, Wu S, Liu H, Stratt R, Barak OG, Shiekhattar R, et al. A novel transcription regulatory
599 complex containing death domain-associated protein and the ATR-X syndrome protein. J Biol Chem.
600 2004 May 7;279(19):20369–77.
601 30. Porter SS, Stepp WH, Stamos JD, McBride AA. Host cell restriction factors that limit
602 transcription and replication of human papillomavirus. Virus Res. 2017 Mar 2;231:10–20.
603 31. Maillet S, Fernandez J, Decourcelle M, El Koulali K, Blanchet FP, Arhel NJ, et al. Daxx
604 Inhibits HIV-1 Reverse Transcription and Uncoating in a SUMO-Dependent Manner. Viruses. 2020
605 Jun 11;12(6).
606 32. Dutrieux J, Maarifi G, Portilho DM, Arhel NJ, Chelbi-Alix MK, Nisole S. PML/TRIM19-
607 Dependent Inhibition of Retroviral Reverse-Transcription by Daxx. PLoS Pathog. 2015
608 Nov;11(11):e1005280.
609 33. OhAinle M, Helms L, Vermeire J, Roesch F, Humes D, Basom R, et al. A virus-packageable
610 CRISPR screen identifies host factors mediating interferon inhibition of HIV. eLife. 2018 Dec
611 6;7:e39823.
612 34. Li W, Xu H, Xiao T, Cong L, Love MI, Zhang F, et al. MAGeCK enables robust identification
613 of essential genes from genome-scale CRISPR/Cas9 knockout screens. Genome Biol. 2014 Dec
614 5;15(12):554.
615 35. Katopodis P, Anikin V, Randeva HS, Spandidos DA, Chatha K, Kyrou I, et al. Pan-cancer
616 analysis of transmembrane protease serine 2 and cathepsin L that mediate cellular SARS-CoV-2
617 infection leading to COVID-19. Int J Oncol. 2020 Aug;57(2):533–9.
618 36. Malakhova OA, Yan M, Malakhov MP, Yuan Y, Ritchie KJ, Kim KI, et al. Protein ISGylation
619 modulates the JAK-STAT signaling pathway. Genes Dev. 2003 Feb 15;17(4):455–60.
620 37. Broering R, Zhang X, Kottilil S, Trippler M, Jiang M, Lu M, et al. The interferon stimulated
621 gene 15 functions as a proviral factor for the hepatitis C virus and as a regulator of the IFN response.
622 Gut. 2010 Aug;59(8):1111–9.
623 38. McLaren PJ, Gawanbacht A, Pyndiah N, Krapp C, Hotter D, Kluge SF, et al. Identification of
624 potential HIV restriction factors by combining evolutionary genomic signatures with functional
625 analyses. Retrovirology. 2015 May 16;12:41.
626 39. Richardson RB, Ohlson MB, Eitson JL, Kumar A, McDougal MB, Boys IN, et al. A CRISPR
627 screen identifies IFI6 as an ER-resident interferon effector that blocks flavivirus replication. Nat
628 Microbiol. 2018 Nov;3(11):1214–23.
629 40. Merkl PE, Orzalli MH, Knipe DM. Mechanisms of Host IFI16, PML, and Daxx Protein
630 Restriction of Herpes Simplex Virus 1 Replication. J Virol. 2018 May 15;92(10).
631 41. Jacquet S, Pontier D, Etienne L. Rapid Evolution of HERC6 and Duplication of a Chimeric
632 HERC5/6 Gene in Rodents and Bats Suggest an Overlooked Role of HERCs in Mammalian Immunity.
633 Front Immunol. 2020;11:605270.
634 42. Liao M, Liu Y, Yuan J, Wen Y, Xu G, Zhao J, et al. Single-cell landscape of bronchoalveolar
635 immune cells in patients with COVID-19. Nat Med. 2020 Jun 1;26(6):842–4.
636 43. Haugh KA, Shalginskikh N, Nogusa S, Skalka AM, Katz RA, Balachandran S. The interferon-
637 inducible antiviral protein Daxx is not essential for interferon-mediated protection against avian
638 sarcoma virus. Virol J. 2014 May 28;11:100.
639 44. Guo K, Barrett BS, Mickens KL, Hasenkrug KJ, Santiago ML. Interferon Resistance of
640 Emerging SARS-CoV-2 Variants. BioRxiv Prepr Serv Biol. 2021 Mar 21;
641 45. Maillet S, Nisole S. Daxx, a broad-spectrum viral restriction factor. Virol Montrouge Fr. 2016
642 Oct 1;20(5):261–72.
643 46. Kuo H-Y, Chang C-C, Jeng J-C, Hu H-M, Lin D-Y, Maul GG, et al. SUMO modification
644 negatively modulates the transcriptional activity of CREB-binding protein via the recruitment of Daxx.
645 Proc Natl Acad Sci U S A. 2005 Nov 22;102(47):16973–8.

646 47. Shih H-M, Chang C-C, Kuo H-Y, Lin D-Y. Daxx mediates SUMO-dependent transcriptional
647 control and subnuclear compartmentalization. Biochem Soc Trans. 2007 Dec;35(Pt 6):1397–400.
648 48. Sudharsan R, Azuma Y. The SUMO ligase PIAS1 regulates UV-induced apoptosis by
649 recruiting Daxx to SUMOylated foci. J Cell Sci. 2012 Dec 1;125(Pt 23):5819–29.
650 49. Jang M-S, Ryu S-W, Kim E. Modification of Daxx by small ubiquitin-related modifier-1.
651 Biochem Biophys Res Commun. 2002 Jul 12;295(2):495–500.
652 50. Lin D-Y, Huang Y-S, Jeng J-C, Kuo H-Y, Chang C-C, Chao T-T, et al. Role of SUMO-
653 interacting motif in Daxx SUMO modification, subnuclear localization, and repression of sumoylated
654 transcription factors. Mol Cell. 2006 Nov 3;24(3):341–54.
655 51. Xie X, Muruato A, Lokugamage KG, Narayanan K, Zhang X, Zou J, et al. An Infectious cDNA
656 Clone of SARS-CoV-2. Cell Host Microbe. 2020 May 13;27(5):841-848.e3.
657 52. Liu G, Lee J-H, Parker ZM, Acharya D, Chiang JJ, van Gent M, et al. ISG15-dependent
658 activation of the sensor MDA5 is antagonized by the SARS-CoV-2 papain-like protease to evade host
659 innate immunity. Nat Microbiol. 2021 Apr;6(4):467–78.
660 53. Shin D, Mukherjee R, Grewe D, Bojkova D, Baek K, Bhattacharya A, et al. Papain-like
661 protease regulates SARS-CoV-2 viral spread and innate immunity. Nature. 2020 Nov;587(7835):657–
662 62.
663 54. Saiz M, Martinez-Salas E. Uncovering targets of the Leader protease: Linking RNA-mediated
664 pathways and antiviral defense. Wiley Interdiscip Rev RNA. 2021 Feb 18;e1645.
665 55. Shaw AE, Hughes J, Gu Q, Behdenna A, Singer JB, Dennis T, et al. Fundamental properties of
666 the mammalian innate immune system revealed by multispecies comparison of type I interferon
667 responses. PLoS Biol. 2017 Dec 18;15(12):e2004086–e2004086.
668 56. Schreiner S, Bürck C, Glass M, Groitl P, Wimmer P, Kinkley S, et al. Control of human
669 adenovirus type 5 gene expression by cellular Daxx/ATRX chromatin-associated complexes. Nucleic
670 Acids Res. 2013 Apr 1;41(6):3532–50.
671 57. Guion LG, Sapp M. The Role of Promyelocytic Leukemia Nuclear Bodies During HPV
672 Infection. Front Cell Infect Microbiol. 2020;10:35.
673 58. Martin M. Cutadapt removes adapter sequences from high-throughput sequencing reads.
674 EMBnet.journal. 2011 May 2;17(1):10.
675 59. Langmead B, Salzberg SL. Fast gapped-read alignment with Bowtie 2. Nat Methods. 2012
676 Apr;9(4):357–9.
677 60. Li H, Handsaker B, Wysoker A, Fennell T, Ruan J, Homer N, et al. The Sequence
678 Alignment/Map format and SAMtools. Bioinforma Oxf Engl. 2009 Aug 15;25(16):2078–9.
679 61. Hsiau T, Conant D, Rossi N, Maures T, Waite K, Yang J, et al. Inference of CRISPR Edits from
680 Sanger Trace Data. bioRxiv. 2019 Jan 1;251082.
681 62. Le T, Phan T, Pham M, Tran D, Lam L, Nguyen T, et al. BBrowser: Making single-cell data
682 easily accessible. bioRxiv. 2020 Jan 1;2020.12.11.414136.